HHS Public Access

Author manuscript

Bone. Author manuscript; available in PMC 2019 July 01.

Published in final edited form as:

Bone. 2018 July ; 112: 58–70. doi:10.1016/j.bone.2018.04.013.

BBS9 gene in nonsyndromic craniosynostosis: role of the primary cilium in the aberrant ossification of the suture osteogenic niche

Marta Barba[1,*], **Lorena Di Pietro**[1,*], **Luca Massimi**[2,3], **Maria Concetta Geloso**[1], **Paolo Frassanito**[3], **Massimo Caldarelli**[2,3], **Fabrizio Michetti**[1], **Stefano Della Longa**[4], **Paul A. Romitti**[5], **Concezio Di Rocco**[6], **Alessandro Arcovito**[7], **Ornella Parolini**[1,8], **Gianpiero Tamburrini**[2,3], **Camilla Bernardini**[1], **Simeon Antonov Boyadjiev**[9,§], and **Wanda Lattanzi**[1,§]

[1]Insitute of Anatomy and Cell Biology, Università Cattolica del Sacro Cuore, 00168, Rome, Italy

[2]Institute of Neurosurgery, Università Cattolica del Sacro Cuore, 00168 Rome, Italy

[3]Fondazione Policlinico Universitario Agostino Gemelli, Largo Gemelli, 1 – 00168 Rome, Italy

[4]Department of Life, Health and Environmental Sciences, University of L'Aquila, 67100, L'Aquila, Italy

[5]Department of Epidemiology, College of Public Health, University of Iowa, Iowa City, 52242, IA, USA

[6]Department of Neurosurgery, International Neuroscience Institute, 30625, Hannover, Germany

[7]Institute of Biochemistry and Clinical Biochemistry, Università Cattolica del Sacro Cuore, 00168, Rome, Italy

[8]Centro di Ricerca E. Menni, Fondazione Poliambulanza-Istituto Ospedaliero, 25124, Brescia, Italy

[9]Section of Genomics, Department of Pediatrics, University of California, 95817, Sacramento, California, USA

Abstract

Nonsyndromic craniosynostosis (NCS) is the premature ossification of skull sutures, without associated clinical features. Mutations in several genes account for a small number of NCS patients; thus, the molecular etiopathogenesis of NCS remains largely unclear.

Our study aimed at characterizing the molecular signaling implicated in the aberrant ossification of sutures in NCS patients. Comparative gene expression profiling of NCS patient sutures

Corresponding author: Wanda Lattanzi, Assistant Professor, Inst. Anatomy and Cell Biology - Università Cattolica del Sacro Cuore, Largo F. Vito, 1, 00168 Rome, Italy, Lab Phone: (+39)0630154464 wanda.lattanzi@unicatt.it.

*MB and LDP contributed equally;

§SAB and WL share senior authorship.

Disclosure statement: The authors have nothing to disclose.

identified a fused suture-specific signature, including 17 genes involved in primary cilium signaling and assembly. Cells from fused sutures displayed a reduced potential to form primary cilia compared to cells from control patent sutures of the same patient. We identified specific upregulated splice variants of the Bardet Biedl syndrome-associated gene 9 (*BBS9*), which encodes a structural component of the ciliary BBSome complex. *BBS9* expression increased during *in vitro* osteogenic differentiation of suture-derived mesenchymal cells of NCS patients. Also, *Bbs9* expression increased during *in vivo* ossification of rat sutures. *BBS9* functional knockdown affected the expression of primary cilia on patient suture cells and their osteogenic potential. Computational modeling of the upregulated protein isoforms (observed in patients) predicted that their binding affinity within the BBSome may be affected, providing a possible explanation for the aberrant suture ossification in NCS.

Keywords

BBS9; osteogenic niche; mesenchymal stromal cells; nonsyndromic craniosynostosis; primary cilium; gene expression signatures

1. Introduction

Craniosynostosis (CS) is a major structural birth defect resulting from premature fusion of one or more skull sutures, and represents the second most common craniofacial defect in humans (after cleft lip/palate), with an overall prevalence of 1/2,000–2,500 live births [1,2]. Although CS is a feature in more than 180 Mendelian syndromes and chromosomal anomalies, most patients (75%–85%) present with a nonsyndromic (isolated) phenotype [3–5].

Nonsyndromic craniosynostosis (NCS) is considered a multifactorial disorder, in which gene-gene and/or gene-environment interaction effects are plausibly involved [5]. NCS subtypes are classified according to the site of premature suture fusion and are named after the consequent abnormal morphology of the skull. Single-suture CS subtypes (suture) include scaphocephaly (sagittal), trigonocephaly (metopic), anterior plagiocephaly (coronal) and posterior plagiocephaly (lambdoid). When multiple sutures are involved, the CS is considered complex and is more likely to be a feature of a syndromic phenotype [6,7].

Although the occurrence of NCS is thought to be largely sporadic, familial recurrence has been reported in 2–10% of patients, suggesting a Mendelian inheritance [5,6,8].

Nonetheless, the genetic etiology of NCS remains largely unclear. Suggested mechanisms include low penetrance of mutations in genes associated with syndromic forms of CS (*FGFR1*, *FGFR2*, *FGFR3*, *TWIST1*, *EFNB1, TCF12*, among others) [4] and mutations in genes acting within interconnected signaling pathways, including *TCF12* [9], *ERF* [10], *TWIST1* [11], *ALX4* [12], *RUNX2* [13], *FREM1* [14] and *ZIC1* [15]. Exposure to environmental risk factors is also considered among the etiopathogenetic events in NCS, also in the light of recent changes in the incidence of different forms [4,16,17]. More recently, two-loci inheritance has been proposed, involving a common risk allele near the *BMP2* locus that increases the penetrance of rare loss of function mutations in *SMAD6* [18].

Even with this evidence, mutations defining a strong genetic etiology for NCS have been reported in a limited proportion of patients [6]. Most NCS appears to occur in the absence of an identifiable underlying cause, suggesting that during skull development, a single suture undergoes an abnormal morphogenesis leading to premature ossification and fusion. This abnormal morphogenesis may be attributed, in part, to local somatic alteration that affects the prematurely fused suture site [19,20].

The results of comparative gene expression profiling between fused and unfused suture tissues and/or cells performed in previous studies, tend to support the hypothesis of local molecular differences acting at the dysmorphic skull site of NCS patients [21–26]. Nonetheless, the data obtained in these studies are poorly comparable and reproducible, largely due to the different experimental designs and protocols used [4,27,28].

To understand the molecular etiology of NCS, we previously performed a genome-wide association study of 130 case-parent trios with sagittal NCS and identified strong and reproducible associations with the *BMP2* and the *BBS9* loci [29]. *BMP2* encodes a member of the TGFβ superfamily and a key growth factor regulating osteoblast development [30]. The TGFβ/BMP and FGF pathways intensely interact during development and osteogenesis, playing pivotal roles in cranial morphogenesis of vertebrates [5,31]. We previously demonstrated that prematurely fused sutures and osteogenic precursors (calvarial-derived mesenchymal cells, CMSC) of sporadic CS patients displayed a constitutive activation of *BMP2* and its downstream osteogenic cascade [32].

With regard to *BBS9*, this gene encodes a structural protein involved in the assembly of a multimeric complex, namely the BBSome, acting in primary cilium biogenesis and intraciliary trafficking [33–36]. *BBS9* initially was identified as a gene downregulated by parathyroid hormone in osteoblasts [37], although its role in the osteogenic signaling has not been well elucidated. *BBS9* loss-of-function mutations are associated with the Bardet-Biedl syndrome (OMIM: #615986), which does not manifest with CS [38].

Although the molecular signaling within the primary cilium has been recognized as a key functional player in craniofacial morphogenesis, to date, a specific role for *BBS9* in CS etiopathogenesis has not been supported by functional evidence. In this study, we have examined the molecular signaling acting in the calvaria of patients affected by NCS, focusing on the functional role of *BBS9* and related primary cilium signaling. We performed comparative molecular and morphological analyses on matched fused/unfused sutures of affected patients, and on cells isolated thereof. *BBS9* knockdown was performed in fused-suture derived cells to validate the functional involvement of this gene in the osteogenic process, and *Bbs9* expression was analyzed in rats during postnatal skull growth, to confirm its implication during *in vivo* suture ossification. Finally, we attempted to identify the contribution of different splice variants encoding alternative BBS9 protein isoforms using computational modeling and correlating the prediction of three-dimensional structure with their functional activity in modeling the assembly of the BBSome.

2. Materials and Methods

2.1 Patient sample and specimen collection

We enrolled a sample of 16 patients affected by midline (sagittal or metopic) NCS following collection of written informed consent from their parents. Patients were of both sexes and aged 3-to-12 months (mean age 6.7±2.4 months, median age 6 months). Detailed patient data, including craniometrics measures and specimen descriptions are provided in Supplemental Table 1. Hotspot CS mutations were excluded by Sanger sequencing analysis of the fibroblast growth factor receptor -1, -2 and -3 (*FGFR1-3*), and in the twist homolog 1 (*TWIST1*) genes.

Suture tissue specimens were collected from patients as surgical waste resulting from cranial remodeling. Specifically, four tissue specimens were collected from each patient: two from the physiological patent suture (termed “Normal”, N) and two from the prematurely fused suture (termed “Pathologic”, P). Two samples (one N and one P) were collected in culture medium and served for cell isolation, the remaining two samples were snap-frozen in liquid nitrogen and served for RNA isolation. The collection site for N and P specimens from each patient is specified in Supplemental Table 1.

Our study protocol was designed according to the European Good Clinical Practice guidelines and with the current revision of the Declaration of Helsinki, and was approved by the Ethical Committee of the *Università Cattolica del Sacro Cuore*, School of Medicine (protocols number A/606/CE/2010 and 19056/14).

2.2 Tissue RNA isolation

Snap-frozen calvarial tissue specimens were grinded using a mortar and pestel and lysed using TRIzol Reagent (Invitrogen, Carlsbad, CA, USA). The phenol-chloroform phase was recovered for protein extraction, as described below. Total RNA was isolated from the aqueous phase and subsequently purified using silica membrane spin columns from RNeasy Mini kit (Qiagen, Chatsworth, CA), as previously described [32]. The yield, quality, and integrity of RNA were determined using the Agilent 2100 Bioanalyzer (Agilent Technologies, Palo Alto, CA, USA), as previously described [27].

2.3 Microarray analysis

Total RNA isolated from selected tissue specimens (Supplemental Table 1) was used as a template to produce libraries of biotinylated cRNAs [39] and hybridized on GeneChips Exon 1.0 ST human microarrays (Affymetrix, Santa Clara, CA, USA), following the procedure described by the manufacturer. This microarray technology implemented a whole-transcript coverage probeset design to enable expression analysis at both the gene and single exon levels.

Data analysis was performed using the Affymetrix® Transcriptome Analysis Console (TAC) Software 3.0, (www.affymetrix.com/estore/browse/level_seven_software_products_only.jsp?productId=prod760001#1_1). Starting from the CEL files, CHP files were generated through the AffymetrixR Expression Console Software; thus, the list of differentially expressed

genes was generated by importing non-paired CHP files and applying a One-Way Between-Subject Analysis of Variance Analysis (ANOVA) p-value threshold ≤0.05 together with an absolute log2 (fold change in linear space) threshold of 1.5.

The exon-level differential expression analysis, which enables distinguishing different isoforms of each gene, was performed by the TAC Software selecting a One-Way Between-Subject ANOVA p-value threshold ≤0.05, and a log2 (fold change in linear space) threshold of 2.

The gene lists underwent biological interpretation according to Gene Ontology enrichment and gene network analysis (by STRING; https://string-db.org/), enabling the definition and prioritization of functional categories. The functional enrichment of the gene lists was implemented using the Database for Annotation, Visualization, and Integrated Discovery (DAVID; http://david.abcc.ncifcrf.gov/) [40].

Our dataset described in this publication was deposited in the NCBI Gene Expression Omnibus (https://www.ncbi.nlm.nih.gov/geo/) [41] and is accessible through the GEO Series Accession Number GSE79386.

2.4 Cells isolation and culture

All reagents were purchased from Euroclone (Milan, Italy). CMSC were isolated in primary culture from each suture tissue specimen harvested from patients, as previously described [32]. This procedure allowed selecting adherent cells isolated from the flat bone boundary at the site of suture, regardless of the suture ossification status. These cells displayed the immunophenotype and biological features (including multilineage potential) of mesenchymal stromal cells, as previously described [32]. Upon confluence, primary cells were detached with trypsin/EDTA and split into two aliquots; one aliquot was plated in T75 flasks and amplified for further experiments, and the other aliquot was stored at −80°C until used for RNA and protein isolation, as described below.

2.5 *In vitro* osteogenic assay

The osteogenic potential of CMSC was analyzed comparatively in cells isolated from N- and P- sutures. Cells were cultured for 5 days in osteogenic medium (OM) [42]. Cells cultured in standard growth medium were used as negative controls for differentiation. Osteogenic differentiation was assessed morphologically using Alizarin red staining and analyzing the expression of osteospecific genes, namely osterix (*OSX*) and alkaline phosphatase (*ALP*), by quantitative real time PCR (qPCR) [43].

2.6 RNA isolation from cells

Total RNA was isolated from CMSC using the RNeasy mini kit (Qiagen, Hilden, Germany), according to the manufacturer's suggested procedures. An additional on-column DNase incubation step was performed, allowing the selective removal of genomic DNA during the isolation process. RNA was quantified using a UV spectrophotometer, and RNA quality and integrity was assessed using the Agilent 2100 Byoanalyzer (Agilent, Santa Clara, CA, USA).

2.7 Quantitative Real Time PCR (qPCR)

The differential expression of *BBS9* and its transcript isoforms was validated, first in tissue specimens, and then in N- and P-CMSC isolated from an independent set of NCS patients using qPCR [42,44]. Sequence-specific oligonucleotide primers were designed to amplify selected *BBS9* isoforms, based on the sequence of the Probe Selection Region (PSR) and Junction Probe Sets sequences of the Exon array. qPCR was also exploited to analyze the expression of the Hedgehog (HH) pathway-related genes, Smoothened (*SMO*) and GLI family zinc finger 1 (*GLI1*) [45,46], to evaluate the primary cilium-related signaling during the osteogenic differentiation of CMSC. The sequences of all oligonucleotide primers used in this study are provided in Supplemental Table 2.

2.8 *BBS9*-silencing

To evaluate the functional role of the *BBS9* gene during osteogenic differentiation, we knocked-down *BBS9* expression in P-CMSC, using a pool of custom-designed double-stranded short interfering RNAs (siRNA) (Qiagen). The sequences of the siRNA constructs are provided in Supplemental Table 3. CMSC were plated in 24-well plates at a density of 2×10^4 cells/well and incubated under standard growth conditions. On the following day, the siRNA constructs were transfected into adherent cells using the HiPerfect® Transfection Reagent (Qiagen), according to the manufacturer's suggested procedure. Cells transfected with AllStars Negative Control siRNA (Qiagen) and cells treated with transfection reagent served as siRNA controls and negative controls, respectively. The efficiency of the silencing was evaluated by analyzing the expression of *BBS9* by qPCR, as previously described [32]. *BBS9*-silenced cells were used in time course experiments of expression analysis and confocal microscopy.

2.9 Cell immunofluorescence (IF)

Immunofluorescence and confocal microscopy analysis was carried out on CMSC to visualize and quantify the expression of BBS9. To this aim cells were incubated with a polyclonal antibody raised against a peptide mapping within an internal region of BBS9 of human origin (BBS9: sc-82536; Santa Cruz Biotecnology, Heidelberg, Germany), combined with a monoclonal antibody against α-acetylated tubulin (αAcTub-Ab; Sigma Aldrich). After incubation with the appropriate fluorophore-associated secondary Ab (1:200), and TO-PRO3 iodide (Life Technologies) counterstaining, all slides were analyzed using the LSM 510 META confocal laser scanning microscopy system (Zeiss, Oberkochen, Germany). At least ten fields representing each slide were examined for each condition. The quantification of the BBS9 fluorescence intensity was performed by the Java image processing and analysis program ImageJ (NIH- https://imagej.nih.gov/ij/download.html) [47].

Immunofluorescence and confocal microscopy analysis was carried out on CMSC, also, to visualize and count the primary cilia. Two protocols were used. The first protocol combined two monoclonal antibodies against α-acetylated tubulin (αAcTub-Ab; Sigma Aldrich) and γ tubulin (γTub-Ab, Sigma Aldrich) to label the shaft and the basal body of the cilium, respectively [48], and allowed assessing cilium structural integrity and position at an improved resolution. The second protocol was implemented to improve the specificity of primary cilium staining over the cytoskeleton, being based on a monoclonal Ab against the

ADP-ribosylation factor-like GTPase 13B (ARL13B; Santa Cruz Biotechnology) expressed selectively inside the cilium [49]. After incubation with the appropriate fluorophore-associated secondary Ab (1:200), and TO-PRO3 iodide (Life Technologies) counterstaining, all slides were analyzed using the LSM 510 META confocal laser scanning microscopy system (Zeiss, Oberkochen, Germany). At least ten fields representing each slide were examined for each condition. The quantification of primary cilia expression was performed on nucleated cells and expressed as percentage of primary cilia per counted nuclei. At least 50 nucleated cells were counted for each tested specimen.

2.10 HH signaling modulation

In order to better evaluate the involvement of the HH signaling in the calvarial sutures closure, the HH activity was modulated by treating N- and P-CMSC cultures with either the agonist purmorphamine or the inhibitor cyclopamine (both purchased from Santa Cruz Biotecnology) [50–52]. To this aim, scalar concentrations (1-2-5 μM) of purmorphamine and cyclopamine were added, alternatively, to both growth and differentiation culture medium, to select the most effective treatment conditions. After these preliminary tests, both chemicals were used at a final concentration of 5μM in growth and differentiation medium, to treat both N- and P-CMSC. Cells cultured in growth and differentiation medium were used as control. All cells were collected 5 days after the treatment. The effect of chemical modulation of HH signaling was evaluated by analyzing *GLI1* expression levels by qPCR, as described elsewhere [45,46].

2.11 *In vivo* BBS9 characterization

Twenty-Five Wistar neonatal rats were used for morphological and molecular studies. The animals were sacrificed through decapitation after the induction of deep anesthesia by hypothermia at postnatal days 1- 4- 7- 14 and 21 (5 animals per time point). The skulls were completely exposed by removing skin, eyes, and soft tissues. For the morphological study, the skull specimens were fixed in 4% paraformaldehyde and double-stained with alcian blue and Alizarin red [53] for connective tissue and bone tissue parts detection, respectively. For the molecular study, sagittal sutures were collected from the skulls immediately after sacrifice and snap-frozen in liquid nitrogen for subsequent RNA isolation. The molecular study was conducted following the protocol described above.

2.12 Statistical Analysis

Data were analyzed using GraphPad Prism software version 6.0. Results are presented as means ± standard deviation (SD). Statistical differences between groups were analyzed using the unpaired Student’s t-test. All statistics were two-tailed and the level of significance was set at $P<0.05$.

2.13 *In silico* analysis of BBS9 domains

The models of the human BBS9 C-terminal domains were built using I-TASSER (https://zhanglab.ccmb.med.umich.edu/I-TASSER/) [54–56]. The secondary structures obtained through I-TASSER were aligned by UCSF Chimera 1.12rc (http://www.rbvi.ucsf.edu/chimera) [57].

3. Results

3.1 Microarray analysis

Microarray analysis was performed to compare the genome-wide expression profiles of matched fused (pathological=P) and unfused (normal=N) suture specimens of 8 patients (Supplemental Table 1). Data analysis was performed both at the gene level and at the single exon level to detect differential expression of transcripts and splice isoforms. The comparison was made between patient-matched fused-versus-non fused sutures, with the precise aim of excluding individual variability and considering the differences due to the pathological event (i.e. premature fusion). This approach allowed evaluating differences in the functional activity (i.e. expression) of genes reflecting the somatic alteration occurring at the site of premature suture fusion, rather than those related to different genetic backgrounds.

3.1.1 Gene-level analysis results—The gene-level microarray analysis, allowed detecting 256 transcripts differentially expressed (242 overexpressed and 14 downregulated genes; $p<0.05$) in P versus N sutures. The extended list of differentially expressed genes is provided in Supplemental File 1. Network analysis and an in-depth literature search allowed identifying 100 upregulated genes involved in bone-related functions (Supplemental File 4), largely interacting in an extended network (STRING-gene level Figure in Supplemental File 4).

The functional enrichment of our gene list, based on Gene Ontology (GO) annotations, enabled identifying core biological functions that appeared to be coherently activated in P-sutures compared with N-sutures (see tables in Supplemental File 4). The top 10 biological process annotations for these genes included cell differentiation, and morphogenetic and developmental processes. The molecular functions and cellular locations resulting from GO enrichment indicated a main representation of molecules involved in binding activities occurring on plasma membranes and in the extracellular space (see Supplemental File 4).

3.1.2 Exon-level analysis results—The exon-level analysis allowed detecting 3066 exons, corresponding to 1573 different transcript clusters, whose expression was significantly different (2918 overexpressed and 148 downregulated; $p<0.05$; supplemental File 5) in P-versus-N suture specimens. Nearly 200 genes in the exon-level list overlapped with those featured in the gene-level list (Figure 1A).

According to GO functional annotations, this gene list includes functional categories related to the extracellular matrix (ECM) organization and cell adhesion (see Gene Ontology in Supplemental File 5). In particular, genes belonging to the collagen and laminin families, responsible for the structural and adhesive properties of the ECM, were overexpressed in P specimens. Moreover, according to the ‘cellular compartment’ GO enrichment, most genes showing differentially expressed exons between P and N specimens, are expressed within the plasma membrane and the extracellular compartments, 19 specifically annotated within the primary cilium compartment. Cilium morphogenesis and assembly were also featured among the most significant categories resulting from ‘biological processes’ annotations (Supplemental File 5).

3.2 Aberrant primary cilium morphology and signaling in prematurely fused sutures of NCS

The biological interpretation of gene- and exon-level lists obtained by TAC analysis (Supplemental File 4 and Supplemental File 5) included 15 dysregulated genes (Supplemental Table 6) that were already described as either confirmed or putative candidates for clinical phenotypes featuring CS [5,58]. Moreover, 17 genes were indexed in the Ciliome Database (http://www.sfu.ca/~leroux/ciliome_database.htm) (Figure 1A; genelist in Supplemental Table 7), which categorizes 114 genes to date. We therefore chose to focus on primary cilium-associated genes, in light of the leading role played by the ciliary signaling in craniofacial development, also evidenced by its recent involvement in the molecular etiopathogenesis of CS [59–67].

The possible qualitative and quantitative abnormalities affecting the primary cilium were investigated in calvarial-derived mesenchymal cells (CMSC) isolated from P and N suture specimens from an independent set of patients suffering from midline NCS (metopic or sagittal) (Supplemental Table 1). Primary cilia were marked with α-Ac-Tub and γ-Tub (described in Materials and Methods) and evaluated comparatively in N- and P-CMSC through confocal microscopy. A reduction of primary cilia in P-CMSC (Figure 1C) compared with N-CMSC (Figure 1B) was found. Specifically, the percentage of primary cilia-expressing cells was significantly ($p<0.05$) reduced in P- versus N-CMSC (Figure 1H). The proteins involved in cilium assembly in differentiated cells also are responsible for the formation of the mitotic spindle during replicative stages [68]. P-CMSC displayed morphologically aberrant mitoses, with asymmetric (Figure 1E), unipolar (Figure 1F), or tripolar (Figure 1G) spindles, compared with N-CMSC (Figure 1D). The percentage of aberrant spindles was significantly ($p<0.05$) higher in P-versus N-CMSC (Figure 1H).

3.3 BBS9 dysregulation in NCS

3.3.1 Differential BBS9 isoform expression in NCS sutures—The list of the cilium-related dysregulated genes (Supplemental Table 7) included the *BBS9* gene. This gene is downregulated by parathyroid hormone in osteoblastic cells and thought to be involved in parathyroid hormone action in bones; however, the exact function of this gene has not been elucidated. The *BBS9* gene features 16 alternative transcripts (splice variants) according to Ensembl annotations, of which 9 are protein-coding (Figure 2). As mentioned, we reported *BBS9* as a putative candidate for sagittal NCS from our GWAS [29]; therefore, we focused on *BBS9*, in order to provide a functional validation and to possibly explain its role in the molecular pathogenesis of the premature suture fusion occurring in NCS.

Specifically, 31 probes for *BBS9* gene were featured in the human Affymetrix GeneChip® Exon 1.0 ST (list provided in Supplemental Table 8). Our exon-level analysis indicated that three probes (PSR/Junction ID #2996346, #2996330, #2996339) mapping on *BBS9* exons 4, 9, and 10, respectively, were overexpressed in P- versus N-CMSC. None of these probes mapped within the *BBS9* splice isoforms in which exons 4, 9, and 10 or any part of these isoforms are skipped (namely *ENST00000434373*, *ENST00000432983*, *ENST00000442858*, *ENST00000627264*, Figure 2). The remainder of BBS9 specific probes examined were not significantly differentially expressed. Taken together, these data suggest

that the expression of the *ENST00000242067*, *ENST00000355070*, *ENST00000396127*, *ENST00000350941*, and *ENST00000425508* splice isoforms (Figure 2) is selectively overexpressed in the P-CMSC of all tested NCS patients.

3.3.2 BBS9 expression profiling in suture-derived cells—To validate the differential expression of the selected *BBS9* splice isoforms, semi-quantitative PCR (qPCR) in N- and P-CMSC was performed. Sequence-specific oligonucleotide primers were designed to amplify the group of isoforms containing the overexpressed exons highlighted by the Exon Array analysis (*ENST00000242067, ENST00000355070, ENST00000396127, ENST00000350941, ENST00000425508*; Figure 2).

The qPCR analysis performed on matched N-CMSC and P-CMSC confirmed that the expression of *BBS9* was higher in P-CMSC compared to N-CMSC (RQ: 2.92; $p<0.05$, Figure 3A). Immunofluorescence for BBS9 protein expression and cellular localization was assessed in CMSC through confocal microscopy. This revealed that BBS9 staining was discrete with a spot-like distribution in N-CMSC, whereas it appeared diffuse throughout the cytoplasm in P-CMSC (Figure 3B, left panels; quantitative data shown in Figure 3C). Therefore, despite appearing upregulated in P-CMSC, BBS9 was expressed in a non-polarized and grossly disorganized distribution within the cellular cytoplasm, coherent with a non-functional and dysregulated expression, causing the reduced number of cilia in these cells.

3.3.3 BBS9 expression during in vitro osteogenic differentiation—To further investigate the functional involvement of *BBS9* in the osteogenic process, comparative gene expression analysis was performed in N- and P-CMSC induced towards *in vitro* differentiation for 5 days. Upon osteogenic induction, the expression of *BBS9* further increased exclusively in P-CMSC, whereas a slight decrease was observed in committed N-CMSC (Figure 3A). Confocal microscopy allowed detecting an increased intensity of *BBS9* fluorescence in P-CMSC compared with N-CMSC, after 5 days of osteogenic induction (Figure 3B, right panels; quantitative data shown in Figure 3C).

3.3.4 BBS9 expression during in vivo suture ossification—Whole-mount staining of postnatal rat skulls allowed the morphological characterization of suture ossification in time course, with the mineralized bone stained in red and the inter-suture mesenchyme and cartilaginous parts in light blue. As shown in Figure 4, calvarial sutures were clearly opened, as the inter-suture mesenchyme stained in blue is visible in the skulls at postnatal day 1 (p1) and 4 (p4) (Figures 4A and 4B). At the latest time points (p7 to p21), the inter-suture mesenchyme progressively disappears, being thinner and less detectable (Figures 4C–4E). At the same time points, the expression of Bbs9 progressively increased in the rat sagittal suture, in a time-related fashion. In particular, Bbs9 expression showed an increasing trend until p14, when it reached its highest and statistically significant level (RQ: 2.98; $p<0.01$) comparted to all other tested points (Figure 4F).

3.4 Functional characterization of *BBS9: in vitro* knock-down

3.4.1 BBS9 knockdown effects on the osteogenic properties of calvarial osteogenic precursors—To validate the functional involvement of *BBS9* in the regulation of the osteogenic commitment, we knocked-down the gene through siRNA in calvarial cells isolated from P-CMSC. Treatment with the AllStars Negative Control siRNA or the transfection reagent, used as siRNA controls and negative controls, respectively, did not significantly affect the expression of tested genes (data not shown). Therefore, in order to facilitate the representation and analyses of our results, we chose to examine and show the effects of BBS9 knockdown on P-CMSC only compared with both untreated P-CMSC and N-CMSC. qPCR showed that upon siRNA treatment, *BBS9* expression was successfully downregulated by nearly 80% after 48 hours in treated P-CMSC compared with untreated P-CMSC (Figure 5A). No significant difference in *BBS9* expression was found between siRNA-treated P-CMSC (si-P-CMSC) and N-CMSC, suggesting that the gene knockdown efficiently reverted *BBS9* dysregulation to physiologic levels.

The effects of *BBS9* knockdown on the osteogenic potential of cells was then analyzed by morphological evaluation, using Alizarin red staining, and by analyzing the expression of osteospecific genes, namely alkaline phosphatase (*ALP*) and osterix (*OSX*), by qPCR. The differentiation capability of the cells significantly decreased after *BBS9* silencing. In particular, Alizarin red staining performed after 5 days of *in vitro* osteogenic induction, revealed a four-fold reduction of mineralized matrix deposits on the cell monolayer in silenced P-CMSC compared with untreated P-CMSC (Figures 5D and 5E). No significant difference in matrix mineralization was found between si-P-CMSC and N-CMSC, suggesting that *BBS9* knockdown was able to revert the osteogenic potential of cells to a physiologic phenotype.

The expression profiles of *ALP* and *OSX* were analyzed in N-, P-, and si-P-CMSC after 5 days of osteogenic induction. qPCR allowed detecting a significantly increased expression of both genes in P-CMSC induced with differentiation medium compared with untreated P-CMSC, whereas only *ALP* was significantly up regulated in osteo-induced N-CMSC compared to N-CMSC grown in standard medium. In contrast, none of the tested genes appeared significantly modulated in si-P-CMSC following osteogenic commitment (Figures 5B and 5C), confirming that *BBS9* inhibition affected the osteogenic potential of the cells and impaired the responsiveness to osteoinductive stimuli.

3.4.2 BBS9 knockdown effects on primary cilium expression—Given the structural role of *BBS9* in the formation and stabilization of the primary cilium, the expression of this cellular compartment in N- and P-CMSC was explored to detect quantitative and qualitative changes both in standard growth and in osteoinductive conditions. This allowed examined of whether BBS9-siRNA-induced knockdown would affect ciliogenesis in P-CMSC during the *in vitro* osteogenic process.

Confocal microscopy analysis showed that the number of cilia was higher in N-CMSC compared to P-CMSC, in standard growth condition (Figures 6A upper panels, and 6B). After the osteogenic induction, the number of primary cilium expressing cells decreased in N-CMSC, but no significant variation occurred in P-CMSC (Figures 6A lower panels, and

6B). Following the BBS9 silencing, the number of cilia increased in si-P-CMSC compared to P-CMSC, reaching a percentage comparable with N-CMSC. Also, in the presence of osteogenic induction, si-P-CMSC showed a profile similar to N-CMSC. In fact, the percentage of si-P-CMSC expressing primary cilium decreased in the presence of OM, compared with standard growth condition (Figures 6A and 6B).

3.4.3 BBS9 knockdown effects on hedgehog pathway activity—The *HH* gene drives the best characterized signaling pathway acting within the primary cilium in vertebrates [69]. The expression of *HH*-activity markers, *SMO* and *GLI1*, was assessed in cells to detect a possible correlation within *BBS9* dysregulation and cilium activity during the course of *in vitro* osteogenic differentiation. Results indicated a decreased expression of *SMO* and *GLI1* during osteogenic induction in N-CMSC, but not in P-CMSC (Figures 6C and 6D). In si-P-CMSC, the expression of both genes was significantly reduced upon osteogenic induction, similar to control cells. Taken together, these data suggest that the constitutive *BBS9* dysregulation acting in P-CMSC impedes the correct *HH*-signaling response to osteogenic stimuli, which is apparently restored upon *BBS9*-knockdown.

In order to demonstrate that HH pathway responded to external stimuli in our *in vitro* model, we modulated HH signaling in CMSC using an agonist (purmorphamine) and an inhibitor (cyclopamine), alternatively. Our results showed that the expression of the HH signaling marker gene *GLI1* was consistently modulated, in both N- and P-CMSC after 5 days of treatment with either of purmorphamine and cyclopamine, both in standard growth condition (SM) and upon osteogenic induction (OM) (Figure 6E and 6F). In particular, *GLI1* levels were significantly reduced by the cyclopamine treatment and increased following purmorphamine treatment, without significant differences between N- and P-CMSC.

3.5 Differential structural organization of BBS9 proteins

To specifically address the functional implication of the selected splice variants found dysregulated in P-CMSC versus N-CMSC of NCS patients, *in silico* study of the structural organization of the BBS9 protein and its domains was conducted. The full-length *BBS9* isoform (Ensembl Id *ENST00000242067*) encodes a 99kDa-protein (UniProt Id Q3SYG4), which features a well-characterized N-terminal β-propeller domain, spanning residues 1-to-407 plus a C-terminal domain (residues 405-887) [70]. The latter has been, only partly, computationally predicted, as constituted by a domain distantly related to the immunoglobulin (Ig)-like b sandwich fold of the g-adaptin ear (GAE) motif and an a/b platform domain, ending with an α domain (Figure 7A) [71]. The splice variants found overexpressed in our specimens, namely ENST00000242067, ENST00000355070, ENST00000396127, ENST00000350941 and ENST00000425508 are translated into isoforms Q3SYG4-1, -7, -4, 2, and -5, respectively. The analysis of the protein sequences allowed assessing that *BBS9* isoform Q3SYG4-5 lacks the entire C-terminus, whereas isoforms Q3SYG4-2, Q3SYG4-4, and Q3SYG4-7 lack 41, 36, and 5 residues, respectively, within the GAE domain (Figure 7A). We then performed a computational modeling of protein structure, which allowed predicting the -organization of the domains in the different isoforms. The results confirmed that isoform Q3SYG4-1contains the entire GAE domain with six β-strands (Figure 7B), whereas both isoforms Q3SYG4-2 and Q3SYG4-4 lack two

β-strands corresponding to the missing residues (Figure 7C), but keep the main arrangement of β-sheets of the whole domain. Finally, isoform Q3SYG4-7 holds the same folding observed in isoform Q3SYG4-1 (Figure 7C).

4. Discussion

This study provided a novel level of evidence for the implication of the primary cilium signaling, acting at the site of premature suture fusion within the human skull. By focusing specifically on the expression of *BBS9* and its isoforms, our data provide a functional validation for this putative candidate gene, associated with sagittal NCS in our previous GWAS [29].

BBS9, also known as parathyroid hormone-responsive b1 (*PTHB1*), was originally described as downregulated by parathyroid hormone in osteoblastic cells [37], although the specific role for this gene in bone biology and related disorders has yet to be well defined. Homozygous and compound heterozygous loss-of-function mutations in *BBS9* cause a clinical variant of the Bardet-Biedl syndrome (OMIM#615986), characterized by a pleiotropic clinical phenotype, including obesity, retinal degeneration, polydactyly, kidney abnormalities, cognitive impairment, hypertension, and diabetes [72]. In addition, associations with the *BBS9* locus have been described in child obesity [73] and abdominal fat distribution trait [74].

BBS9 encodes a member of the well-characterized class of BBS proteins, seven of which (namely, BBS1, 2, 4, 5, 7, 8, and 9) bind to one another to form an octameric complex (including also the BBSome interacting protein 1, BBIP1), named the BBSome [75]. The BBSome is located at the basal body of the primary cilium and is necessary for ciliogenesis and ciliary function, including sorting membrane proteins to cilia, regulating intraflagellar transport, and modulating sonic hedgehog signal transduction [71,76].

Our results showed that a group of splice isoforms of *BBS9* is overexpressed in fused suture specimens of patients suffering from single-suture midline NCS, compared with same patient-matched unfused suture specimens. We further confirmed this evidence by comparing *BBS9* isoform expression in mesenchymal stromal cells isolated from fused and unfused sutures of patients. The expression of both *BBS9* transcripts and proteins further increased upon *in vitro* osteogenic induction, only in cells isolated from fused suture specimens, suggesting that it might be involved in the aberrant molecular signaling underlying premature suture ossification. Indeed, the transient functional knockdown of *BBS9*, through siRNA, reduced the *in vitro* osteogenic potential of cells isolated from NCS fused sutures. We also have shown that the expression of *Bbs9* tended to increase during postnatal skull suture ossification in rats. Taken together, these data may reasonably allow postulating a direct, though previously undefined, involvement of *BBS9* in bone formation during skull morphogenesis, possibly encompassing its implication in primary cilium formation and signaling.

Recent *in vitro* studies have implicated the primary cilium in mesenchymal stromal cells as both a chemosensor and a mechanosensor, being essential for osteogenic differentiation [77].

Craniofacial phenotypes have been described in established ciliopathies and mutations in ciliary genes have been also described in craniofacial phenotypes previously not categorized as ciliopathies [78]. Specifically, mutations in ciliary genes are found in syndromes that may include CS in their phenotypes, including Sensenbrenner syndrome, Carpenter syndrome, Mainzer–Saldino syndrome, and cranioectodermal dysplasias types 2 and 4 [67,79]. Furthermore, the role of ciliary signaling in CS is corroborated by observation of lambdoid CS in mice with *Gli3* null allele [80].

In this study, mesenchymal stromal cells isolated from fused sutures of NCS patients displayed a dysregulated expression of BBS9 and a reduced tendency to form primary cilia compared with open suture-derived cells from the same patient. Confocal microscopy showed that the excess protein tends to accumulate in the cytoplasm without being polarized in the predicted location of the basal body of the primary cilium. This may suggest that, despite the overall increased *BBS9* expression, the dysregulated splice variants' levels lead to an imbalance of protein isoforms, impairing the correct assembly of functional primary cilia. Upon osteogenic induction, the number of cilia decreased only in control cells, suggesting that, in physiologic conditions, the primary cilium is needed to sense osteoinductive stimuli and transduce them inside the cell to activate the osteogenic cascade. Thereafter, once the process of differentiation is activated, this sensing is not needed anymore; hence, the cilia tend to decrease. A similar trend of dynamic modifications in primary cilium expression have been found to regulate the adipogenic differentiation of mesenchymal stromal cells [46]. Conversely, the number of cilium-expressing cells in specimens derived from fused sutures did not change significantly upon osteogenic induction, suggesting that osteogenic precursors at the pathologic site are not able to sense appropriately environmental stimuli within the growing skull.

The variation in the number of cilia reflected the activity of bone-related signaling pathways active in the cilioplasm, such as that of the HH gene. HH has been shown to be involved in the osteogenic differentiation of mesenchymal stromal cells and is the main signaling cascade within the primary cilium [81–84]. In our model, the expression profiles of *SMO* and *GLI1*, key molecules of HH signaling, indicated that the pathway activity was altered in P-CMSC, during the osteogenic differentiation coherently with the number of primary cilia, as their levels decreased upon osteogenic induction exclusively in control cells. The alteration of HH pathway seemed to mainly depend on the impairment of ciliogenesis, since this signaling properly responded to external stimuli as demonstrated by the effect of chemical modulation induced in suture-derived cells by treatment with either purmorphamine or cyclopamine. It was demonstrated previously that the activation of HH signaling inversely correlated with the osteogenic differentiation of human bone marrow mesenchymal stromal cells [85].

Our results also showed that the physiologic cellular phenotype was restored in fused suture-derived cells upon *BBS9* knockdown, which turned the count of primary cilia and the expression of *SMO* and *GLI1* transcripts, to similar levels than those of control cells, both in standard growth conditions and during osteogenic induction. The mechanism through which *BBS9* exerts its regulatory function in this process could be related to the correct assembly of the BBSome, which is essential for the biogenesis of the primary cilium membrane and

plays a key role in the osteogenic commitment mesenchymal stromal cells [86–88]. Zhang and colleagues reported that BBS9 dysregulation greatly decreases the association of BBS1, BBS4, and BBS8, with BBS2 in the BBSome [35,76]. Nevertheless, a previous study associated the *Bbs9* full-length knockout in zebrafish to the reduction of both number and length of primary cilia [89], without associating it to a clear skull phenotype, either in the zebrafish or in higher vertebrates. Indeed, our work linked the impaired ciliogenesis with the upregulation of only selected BBS9 isoforms, plausibly resulting in the inefficient assembly of the BBSome.

Indeed, the way BBS9 binds its cognates and permits the assemblage of the multimeric BBSome complex involves the C-terminus, which is specifically responsible for protein dimerization [70]. This domain contains a binding site for the Leucine-zipper transcription factor-like 1 protein (LZTFL1), which negatively regulates the ciliary trafficking, particularly affecting the SHH signal transducer SMO, which localizes to the primary cilium [90]. Interestingly, one of the *BBS9* splice variants (*ENST00000425508*) that was overexpressed in fused sutures of NCS patients is translated into a truncated protein missing the entire C-terminal domain, suggesting that this protein isoform could not correctly bind BBS2 and BBS7 during the assembly of the BBSome core complex. Moreover, the secondary structure alignment analysis, showed that two additional isoforms overexpressed in fused sutures, namely *ENST00000396127* and *ENST00000350941*, lack two β-strands in the GAE domain. The GAE motif has been reported as a hotspot for the assembly of the coat complex that sorts membrane proteins to cilia [71]; hence, we hypothesize that the alternative secondary structure of these isoforms may affect ciliary trafficking in fused suture compared with patent suture sites. Further support for this hypothesis comes from our confocal microscopy results, demonstrating that BBS9 expression was de-localized as a diffuse signal throughout the cytoplasm of cells isolated from fused sutures. Conversely, BBS9 immunofluorescence was detectable in the perinuclear region (where the cilium basal body is usually found) of cells isolated from control patent sutures. Taken together, these data suggest that selected BBS9 protein isoforms show a tissue-specific increased expression and activity in osteogenic precursors residing in fused sutures of NCS patients, owing to a less effective assembly of the BBSome, which impairs ciliogenesis. The reduced expression of primary cilia on cells from fused/fusing sutures could reasonably affect their capability to respond to the surrounding environment. This aberrant sensing to external stimuli may lead to a dysregulated and prematurely activated osteogenic process, devoid of appropriate synchronization with the morphogenesis of the whole skull.

4.1 Conclusions

The molecular etiopathogenesis of craniosynostosis entails a complex and heterogeneous network of aberrant signaling cascades leading to the spatiotemporal dysregulation of stimuli inducing, ultimately, excessive and premature osteogenesis of progenitor stromal cells in the skull suture mesenchyme [5,67]. In this context, our study provides original evidence of the active role played by the primary cilium in the regulation of osteogenesis leading to suture fusion, highlighting the *BBS9* gene as a putative key candidate in this process. Furthermore, our results may pave the way to further characterization of the predicted tissue specific BBS9 protein isoforms with different affinity in BBSome binding

and alternative role in ciliary trafficking, which may be specifically involved osteogenesis and premature suture fusion in NCS.

Supplementary Material

Refer to Web version on PubMed Central for supplementary material.

Acknowledgments

We thank Davide Bonvissuto and Enrico Guadagni for their technical support and Paola Leonardi and all the paramedics for patient management. We are extremely grateful to the patients' families who provided their consent to participate in the study.

Financial support: This work was supported in part by: National Institute of Dental and Craniofacial Research, National Institutes of Health (R01 DE016886 to SAB and PAR), *Federazione GENE* nonprofit organization (research grant to WL), and *Università Cattolica del Sacro Cuore* ("linea D1" to WL and to AA).

References

1. Cohen, MJ., MacLean, RE. Craniosynostosis: Diagnosis. Evaluation. and Management. Oxford University Press; New York. NY: 2000.
2. Boyadjiev, SA. Congenital craniofacial abnormalities. Merck Manual 2105. 2014. Available from: http://www.merckmanuals.com/professional/pediatrics/congenital-craniofacial-and-musculoskeletal-abnormalities/congenital-craniofacial-abnormalities
3. Roscioli T, Elakis G, Cox TC, Moon DJ, Venselaar H, Turner AM, et al. Genotype and clinical care correlations in craniosynostosis: findings from a cohort of 630 Australian and New Zealand patients. Am J Med Genet C Semin Med Genet. 2013; 163C:259–70. [PubMed: 24127277]
4. Heuzé Y, Holmes G, Peter I, Richtsmeier JT, Jabs EW. Closing the gap: genetic and genomic continuum from syndromic to nonsyndromic craniosynostoses. Current Genetic Medicine Reports. 2014; 2:135–45. [PubMed: 26146596]
5. Lattanzi W, Barba M, Di Pietro L, Boyadjiev SA. Genetic advances in craniosynostosis. Am J Med Genet A. 2017; 173:1406–29. [PubMed: 28160402]
6. Wilkie AO, Byren JC, Hurst JA, Jayamohan J, Johnson D, Knight SJ, et al. Prevalence and complications of single-gene and chromosomal disorders in craniosynostosis. Pediatrics. 2010; 126:e391–e400. [PubMed: 20643727]
7. Lattanzi W, Bukvic N, Barba M, Tamburrini G, Bernardini C, Michetti F, et al. Genetic basis of single-suture synostoses: Genes. chromosomes and clinical implications. ChildsNervous System. 2012; 28:1301–10.
8. Boyadjiev SA. Genetic analysis of non-syndromic craniosynostosis. Orthod Craniofacial Res. 2007; 10:129–37.
9. Sharma VP, Fenwick AL, Brockop MS, McGowan SJ, Goos JA, Hoogeboom AJ, et al. Mutations in TCF12. encoding a basic helix-loop-helix partner of TWIST1. are a frequent cause of coronal craniosynostosis. Nat Genet. 2013; 45:304–7. [PubMed: 23354436]
10. Twigg SR, Vorgia E, McGowan SJ, Peraki I, Fenwick AL, Sharma VP, et al. Reduced dosage of ERF causes complex craniosynostosis in humans and mice and links ERK1/2 signaling to regulation of osteogenesis. Nat Genet. 2013; 45:308–13. [PubMed: 23354439]
11. Ye X, Guilmatre A, Reva B, Peter I, Heuzé Y, Richtsmeier JT, et al. Mutation screening of candidate genes in patients with nonsyndromic sagittal craniosynostosis. PlastReconstr Surg. 2016; 137:952–61.
12. Dee CT, Szymoniuk CR, Mills PE, Takahashi T. Defective neural crest migration revealed by a Zebrafish model of Alx1-related frontonasal dysplasia. Hum Mol Genet. 2013; 22:239–51. [PubMed: 23059813]

13. Seto ML, Hing AV, Chang J, Hu M, Kapp-Simon KA, Patel PK, et al. Isolated sagittal and coronal craniosynostosis associated with TWIST box mutations. Am J Med Genet A. 2007; 143A:678–86. [PubMed: 17343269]
14. Vissers LE, Cox TC, Maga AM, Short KM, Wiradjaja F, Janssen IM, et al. Heterozygous mutations of FREM1 are associated with an increased risk of isolated metopic craniosynostosis in humans and mice. PLoS Genet. 2011; 7:e1002278. [PubMed: 21931569]
15. Twigg SR, Forecki J, Goos JA, Richardson IC, Hoogeboom AJ, van den Ouweland AM, et al. Gain-of-Function mutations in ZIC1 are associated with Coronal craniosynostosis and learning disability. Am J Hum Genet. 2015; 97:378–88. [PubMed: 26340333]
16. Selber J, Reid RR, Chike-Obi CJ, Sutton LN, Zackai EH, McDonald-McGinn D, et al. The changing epidemiologic spectrum of single-suture synostoses. Plast Reconstr Surg. 2008; 122:527–533. [PubMed: 18626371]
17. van der Meulen J, van der Hulst R, van Adrichem L, Arnaud E, Chin-Shong D, Duncan C, et al. The increase of metopic synostosis: A pan-European observation. J Craniofac Surg. 2009; 20:283–6. [PubMed: 19326483]
18. Timberlake AT, Choi J, Zaidi S, Lu Q, Nelson-Williams C, Brooks ED, et al. Two locus inheritance of non-syndromic midline craniosynostosis via rare SMAD6 and common BMP2 alleles. Elife. 2016; 5:e20125. [PubMed: 27606499]
19. Kim SD, Yagnik G, Cunningham ML, Kim J, Boyadjiev SA. MAPK/ERK signaling pathway analysis in primary osteoblasts from patients with nonsyndromic sagittal craniosynostosis. Cleft Palate Craniofac. 2014; J51:115–9.
20. Al-Rekabi Z, Wheeler MM, Leonard A, Fura AM, Juhlin I, Frazar C, et al. Activation of the IGF1 pathway mediates changes in cellular contractility and motility in single-suture craniosynostosis. J Cell Sci. 2016; 129:483–91. [PubMed: 26659664]
21. Coussens AK, Wilkinson CR, Hughes IP, Morris CP, van Daal A, Anderson PJ, et al. Unravelling the molecular control of calvarial suture fusion in children with craniosynostosis. BMC Genomics. 2007; 8:458. [PubMed: 18076769]
22. Coussens AK, Hughes IP, Wilkinson CR, Morris CP, Anderson PJ, Powell BC, et al. Identification of genes differentially expressed by prematurely fused human sutures using a novel in vivo - in vitro approach. Differentiation. 2008; 76:531–45. [PubMed: 18093228]
23. Coussens AK, Hughes IP, Morris CP, Powell BC, Anderson PJ. In vitro differentiation of human calvarial suture derived cells with and without dexamethasone does not induce in vivo-like expression. J Cell Physiol. 2009; 218:183–91. [PubMed: 18803234]
24. Stamper BD, Park SS, Beyer RP, Bammler TK, Farin FM, Mecham B, et al. Differential expression of extracellular matrix-mediated pathways in single-suture craniosynostosis. PLoS One. 2011; 6:e26557. [PubMed: 22028906]
25. Park SS, Beyer RP, Smyth MD, Clarke CM, Timms AE, Bammler TK, et al. Osteoblast differentiation profiles define sex specific gene expression patterns in craniosynostosis. Bone. 2015; 76:169–76. [PubMed: 25753363]
26. Potter AB, Rhodes JL, Vega RA, Ridder T, Shiang R. Gene expression changes between patent and fused cranial sutures in a nonsyndromic craniosynostosis population. Eplasty. 2015; 15:e12. [PubMed: 25987937]
27. Bernardini C, Barba M, Tamburrini G, Massimi L, Di Rocco C, Michetti F, et al. Gene expression profiling in human craniosynostoses: a tool to investigate the molecular basis of suture ossification. Childs NervSyst. 2012; 28:1295–300.
28. Sanchez-Lara PA. Clinical and Genomic Approaches for the Diagnosis of Craniofacial Disorders. Curr Top Dev Biol. 2015; 115:543–59. [PubMed: 26589937]
29. Justice CM, Yagnik G, Kim Y, Peter I, Jabs EW, Erazo M, et al. A genome-wide association study identifies susceptibility loci for nonsyndromic sagittal craniosynostosis near BMP2 and within BBS9. Nat Genet. 2012; 44:1360–64. [PubMed: 23160099]
30. Rosen V. BMP2 signaling in bone development and repair. Cytokine Growth Factor Rev. 2009; 20:475–80. [PubMed: 19892583]
31. Maxson R, Ishii M. The Bmp pathway in skull vault development. Front Oral Biol. 2008; 12:197–208. [PubMed: 18391502]

32. Lattanzi W, Barba M, Novegno F, Massimi L, Tesori V, Tamburrini G, et al. Lim mineralization protein is involved in the premature calvarial ossification in sporadic craniosynostoses. Bone. 2013; 52:474–84. [PubMed: 22982077]
33. Jin H, Nachury MV. The BBSome. Curr Biol. 2009; 19:R472–73. [PubMed: 19549489]
34. Wei Q, Zhang Y, Li Y, Zhang Q, Ling K, Hu J. The BBSome controls IFT assembly and turnaround in cilia. Nat Cell Biol. 2012; 14:950–57. [PubMed: 22922713]
35. Zhang Q, Yu D, Seo S, Stone EM, Sheffield VC. Intrinsic protein-protein interaction-mediated and chaperonin-assisted sequential assembly of stable bardet-biedl syndrome protein complex. the BBSome. J Biol Chem. 2012; 287:20625–35. [PubMed: 22500027]
36. Mourão A, Christensen ST, Lorentzen E. The intraflagellar transport machinery in ciliary signaling. Curr Opin Struct Biol. 2016; 41:98–108. [PubMed: 27393972]
37. Adams AE, Rosenblatt M, Suva LJ. Identification of a novel parathyroid hormone-responsive gene in human osteoblastic cells. Bone. 1999; 24:305–13. [PubMed: 10221542]
38. Tobin JL, Beales PL. Bardet-Biedl syndrome: beyond the cilium. Pediatr Nephrol. 2007; 22:926–36. [PubMed: 17357787]
39. Lattanzi W, Bernardini C, Gangitano C, Michetti F. Hypoxia-like transcriptional activation in TMT-induced degeneration: microarray expression analysis on PC12 cells. J Neurochem. 2007; 100:1688–1702. [PubMed: 17348866]
40. Sherman BT, Huang da W, Tan Q, Guo Y, Bour S, Liu D, et al. DAVID Knowledgebase: a gene-centered database integrating heterogeneous gene annotation resources to facilitate high-throughput gene functional analysis. BMC Bioinformatics. 2007; 8:426. [PubMed: 17980028]
41. Edgar R, Domrachev M, Lash AE. Gene Expression Omnibus: NCBI gene expression and hybridization array data repository. NucleicAcids Res. 2002; 30:207–10.
42. Barba M, Pirozzi F, Saulnier N, Vitali T, Natale MT, Logroscino G, et al. Lim mineralization protein 3 induces the osteogenic differentiation of human amniotic fluid stromal cells through Kruppel-like factor-4 downregulation and further bone-specific gene expression. J Biomed Biotechnol. 2012; 2012:813894. [PubMed: 23097599]
43. Saulnier N, Lattanzi W, Puglisi MA, Pani G, Barba M, Piscaglia AC, et al. Mesenchymal stromal cells multipotency and plasticity: induction toward the hepatic lineage. Eur Rev Med Pharmacol Sci Suppl. 2009; 1:71–8.
44. Marei HE, Ahmed AE, Michetti F, Pescatori M, Pallini R, Casalbore P, et al. Gene expression profile of adult human olfactory bulb and embryonic neural stem cell suggests distinct signaling pathways and epigenetic control. PLoS One. 2012; 7:e33542. [PubMed: 22485144]
45. Gorojankina T. Hedgehog signaling pathway: a novel model and molecular mechanisms of signal transduction. Cell Mol Life Sci. 2016; 73:1317–32. [PubMed: 26762301]
46. Forcioli-Conti N, Lacas-Gervais S, Dani C, Peraldi P. The primary cilium undergoes dynamic size modifications during adipocyte differentiation of human adipose stem cells. Biochem Biophys Res Commun. 2015; 458:117–22. [PubMed: 25637533]
47. Schneider CA, Rasband WS, Eliceiri KW. NIH Image to ImageJ: 25 years of image analysis. Nat Methods. 2012; 9:671–5. [PubMed: 22930834]
48. Dacheux D, Roger B, Bosc C, Landrein N, Roche E, Chansel L, et al. Human FAM154A (SAXO1) is a microtubule-stabilizing protein specific to cilia and related structures. J Cell Sci. 2015; 128:1294–1307. [PubMed: 25673876]
49. Zhang Q, Hu J, Ling K. Molecular views of Arf-like small GTPases in cilia and ciliopathies. Exp Cell Res. 2013; 319:2316–22. [PubMed: 23548655]
50. Plaisant M, Giorgetti-Peraldi S, Gabrielson M, Loubat A, Dani C, Peraldi P. Inhibition of hedgehog signaling decreases proliferation and clonogenicity of human mesenchymal stem cells. PLoS One. 2011; 6:e16798. [PubMed: 21304817]
51. Oliveira FS, Bellesini LS, Defino HL, da Silva Herrero CF, Beloti MM, Rosa AL. Hedgehog signaling and osteoblast gene expression are regulated by purmorphamine in human mesenchymal stem cells. J Cell Biochem. 2012; 113:204–8. [PubMed: 21898541]
52. Faghihi F, Baghaban Eslaminejad M, Nekookar A, Najar M, Salekdeh GH. The effect of purmorphamine and sirolimus on osteogenic differentiation of human bone marrow-derived mesenchymal stem cells. Biomed Pharmacother. 2013; 67:31–8. [PubMed: 23228449]

53. Bayatli KA, Fadhil SM, Shakir MM. Morpho-histological study of skull bones development in indigenous goose embryo (Anser anser domesticus). IJABR. 2012; 2:469–76.
54. Zhang Y. I-TASSER server for protein 3D structure prediction. BMC Bioinformatics. 2008; 9:40. [PubMed: 18215316]
55. Roy A, Kucukural A, Zhang Y. I-TASSER: a unified platform for automated protein structure and function prediction. Nature Protocols. 2010; 5:725–38. [PubMed: 20360767]
56. Yang J, Yan R, Roy A, Xu D, Poisson J, Zhang Y. The I-TASSER Suite: Protein structure and function prediction. Nat Meth. 2015; 12:7–8.
57. Pettersen EF, Goddard TD, Huang CC, Couch GS, Greenblatt DM, Meng EC, et al. UCSF Chimera--a visualization system for exploratory research and analysis. J Comput Chem. 2004; 25:1605–12. [PubMed: 15264254]
58. Lattanzi, W. eLS. John Wiley&Sons. Ltd; Chichester: 2016. Molecular genetics of craniosynostosis.
59. Silveira KC, Moreno CA, Cavalcanti DP. Beemer-Langer syndrome is a ciliopathy due to biallelic mutations in IFT122. Am J Med Genet A. 2017; 173:1186–1189. [PubMed: 28370949]
60. Schock EN, Struve JN, Chang CF, Williams TJ, Snedeker J, Attia AC, et al. A tissue-specific role for intraflagellar transport genes during craniofacial development. PLoS One. 2017; 12:e0174206. [PubMed: 28346501]
61. Millington G, Elliott KH, Chang YT, Chang CF, Dlugosz A, Brugmann SA. Cilia-dependent GLI processing in neural crest cells is required for tongue development. Dev Biol. 2017; 424:124–137. [PubMed: 28286175]
62. Chang YT, Chaturvedi P, Schock EN, Brugmann SA. Understanding Mechanisms of GLI-Mediated Transcription during Craniofacial Development and Disease Using the Ciliopathic Mutant, talpid(2). Front Physiol. 2016; 7:468. [PubMed: 27799912]
63. Girisha KM, Shukla A, Trujillano D, Bhavani GS, Hebbar M, Kadavigere R, et al. A homozygous nonsense variant in IFT52 is associated with a human skeletal ciliopathy. Clin Genet. 2016; 90:536–539. [PubMed: 26880018]
64. Smith C, Lamont RE, Wade A, Bernier FP, Parboosingh JS, Innes AM. A relatively mild skeletal ciliopathy phenotype consistent with cranioectodermal dysplasia is associated with a homozygous nonsynonymous mutation in WDR35. Am J Med Genet A. 2016; 170:760–5. [PubMed: 26691894]
65. Li Y, Garrod AS, Madan-Khetarpal S, Sreedher G, McGuire M, Yagi H, et al. Respiratory motile cilia dysfunction in a patient with cranioectodermal dysplasia. Am J Med Genet A. 2015; 167A: 2188–96. [PubMed: 25914204]
66. Liu B, Chen S, Johnson C, Helms JA. A ciliopathy with hydrocephalus, isolated craniosynostosis, hypertelorism, and clefting caused by deletion of Kif3a. Reprod Toxicol. 2014; 48:88–97. [PubMed: 24887031]
67. Twigg SR, Wilkie AO. New insights into craniofacial malformations. Hum Mol Genet. 2015; 24:R50–9. [PubMed: 26085576]
68. Goto H, Inaba H, Inagaki M. Mechanisms of ciliogenesis suppression in dividing cells. Cell Mol Life Sci. 2017; 74:881–90. [PubMed: 27669693]
69. Ramsbottom SA, Pownall ME. Regulation of Hedgehog Signalling Inside and Outside the Cell. J Dev Biol. 2016; 4:23. [PubMed: 27547735]
70. Knockenhauer KE, Schwartz TU. Structural Characterization of Bardet-Biedl Syndrome 9 Protein (BBS9). J Biol Chem. 2015; 290:19569–83. [PubMed: 26085087]
71. Jin H, White SR, Shida T, Schulz S, Aguiar M, Gygi SP, et al. The conserved Bardet-Biedl syndrome proteins assemble a coat that traffics membrane proteins to cilia. Cell. 2010; 141:1208–19. [PubMed: 20603001]
72. Benzinou M, Walley A, Lobbens S, Charles MA, Jouret B, Fumeron F, et al. Bardet-Biedl syndrome gene variants are associated with both childhood and adult common obesity in French Caucasians. Diabetes. 2006; 55:2876–82. [PubMed: 17003356]
73. Hendricks AE, Bochukova EG, Marenne G, Keogh JM, Atanassova N, Bounds R, et al. Rare Variant Analysis of Human and Rodent Obesity Genes in Individuals with Severe Childhood Obesity. Sci Rep. 2017; 7:4394. [PubMed: 28663568]

74. Sung YJ, Pérusse L, Sarzynski MA, Fornage M, Sidney S, Sternfeld B, et al. Genome-wide association studies suggest sex-specific loci associated with abdominal and visceral fat. Int J Obes. 2016; 40:662–74.
75. Nachury MV, Loktev AV, Zhang Q, Westlake CJ, Peränen J, Merdes A, et al. A core complex of BBS proteins cooperates with the GTPase Rab8 to promote ciliary membrane biogenesis. Cell. 2007; 129:1201–13. [PubMed: 17574030]
76. Zhang Q, Seo S, Bugge K, Stone EM, Sheffield VC. BBS proteins interact genetically with the IFT pathway to influence SHH-related phenotypes. Hum Mol Genet. 2012; 21:1945–53. [PubMed: 22228099]
77. Chen JC, Hoey DA, Chua M, Bellon R, Jacobs CR. Mechanical signals promote osteogenic fate through a primary cilia-mediated mechanism. FASEB J. 2016; 30:1504–11. [PubMed: 26675708]
78. Zaghloul NA, Brugmann SA. The emerging face of primary cilia. Genesis. 2011; 49:231–46. [PubMed: 21305689]
79. Twigg SR, Wilkie AO. A Genetic-Pathophysiological Framework for Craniosynostosis. Am J Hum Genet. 2015; 97:359–77. [PubMed: 26340332]
80. Rice DP, Connor EC, Veltmaat JM, Lana-Elola E, Veistinen L, Tanimoto Y, et al. Gli3Xt-J/Xt-J mice exhibit lambdoid suture craniosynostosis which results from altered osteoprogenitor proliferation and differentiation. Hum Mol Genet. 2010; 19:3457–67. [PubMed: 20570969]
81. Cai JQ, Huang YZ, Chen XH, Xie HL, Zhu HM, Tang L, et al. Sonic hedgehog enhances the proliferation and osteogenic differentiation of bone marrow-derived mesenchymal stem cells. Cell Biol Int. 2012; 36:349–55. [PubMed: 22149964]
82. Huang C, Tang M, Yehling E, Zhang X. Overexpressing sonic hedgehog peptide restores periosteal bone formation in a murine bone allograft transplantation model. Mol Ther. 2014; 22:430–39. [PubMed: 24089140]
83. James AW, Leucht P, Levi B, Carre AL, Xu Y, Helms JA, Longaker MT. Soni cHedgehog influences the balance of osteogenesis and adipogenesis in mouse adipose-derived stromal cells. Tissue Eng Part A. 2010; 16:2605–16. [PubMed: 20367246]
84. Wang C, Shan S, Wang C, Wang J, Li J, Hu G, et al. Mechanical stimulation promote the osteogenic differentiation of bone marrow stromal cells through epigenetic regulation of Sonic Hedgehog. Exp Cell Res. 2017; 352:346–56. [PubMed: 28215635]
85. Plaisant M, Fontaine C, Cousin W, Rochet N, Dani C, Peraldi P. Activation of hedgehog signaling inhibits osteoblast differentiation of human mesenchymal stem cells. Stem Cells. 2009; 27:703–13. [PubMed: 19096040]
86. Hoey DA, Tormey S, Ramcharan S, O'Brien FJ, Jacobs CR. Primary cilia-mediated mechanotransduction in human mesenchymal stem cells. Stem Cells. 2012; 30:2561–70. [PubMed: 22969057]
87. Bodle JC, Rubenstein CD, Phillips ME, Bernacki SH, Qi J, Banes AJ, et al. Primary cilia: the chemical antenna regulating human adipose-derived stem cell osteogenesis. PLoS One. 2013; 8:e62554. [PubMed: 23690943]
88. Yuan X, Serra RA, Yang S. Function and regulation of primary cilia and intraflagellar transport proteins in the skeleton. Ann N Y Acad Sci. 2015; 1335:78–9. [PubMed: 24961486]
89. Veleri S, Bishop K, Dalle Nogare DE, English MA, Foskett TJ, Chitnis A, et al. Knockdown of Bardet-Biedl syndrome gene BBS9/PTHB1 leads to cilia defects. PLoS One. 2012; 7:e34389. [PubMed: 22479622]
90. Seo S, Zhang Q, Bugge K, Breslow DK, Searby CC, Nachury MV, et al. A novel protein LZTFL1 regulates ciliary trafficking of the BBSome and Smoothened. PLoS Genet. 2011; 7:e1002358. [PubMed: 22072986]

Highlights

- *BBS9* expression is dysregulated in prematurely ossified sutures of craniosynostosis patients
- Primary cilium expression and signaling are abnormal in patient sutures' cells
- A specific *BBS9* splice isoform is overexpressed in prematurely fused sutures
- The resulting BBS9 isoform may be unable to drive the correct assembly of the primary cilium

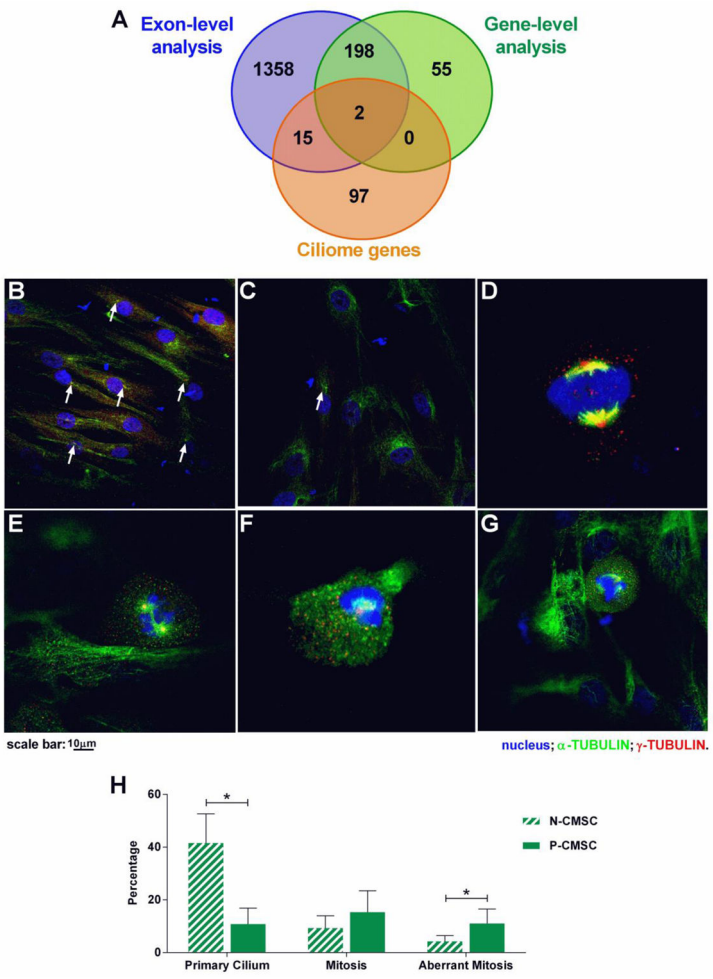

Figure 1. Ciliome genes and primary cilium expression in CMSC

(*A*) The Venn diagram shows the intersection between the microarray gene lists (comprising an overall number of 200 genes, listed in Supplemental Files 4 and 5) and the 297 genes annotated in the ciliome database: 17 genes (listed in Supplemental Table 4) are shared between the three groups. Confocal microscopy on IF slides allowed detecting the expression of primary cilium (arrows) on cells isolated from unfused suture (*B*) and on cells from fused suture (*C*), along with the regularly shaped mitotic spindle in N-CMSC (*D*), and the aberrant spindles in P-CMSC (monopolar spindle in *E*, asymmetric spindle in *F* and tripolar spindle in *G*). Quantitative data expressed in percentage are shown in *H*: proportion of primary cilium-expressing cells, and of normal/aberrant mitotic spindles, in N-CMSC compared with P-CMSC. Unpaired t-test was used to detect the statistical significance between samples; *p≤0.05.

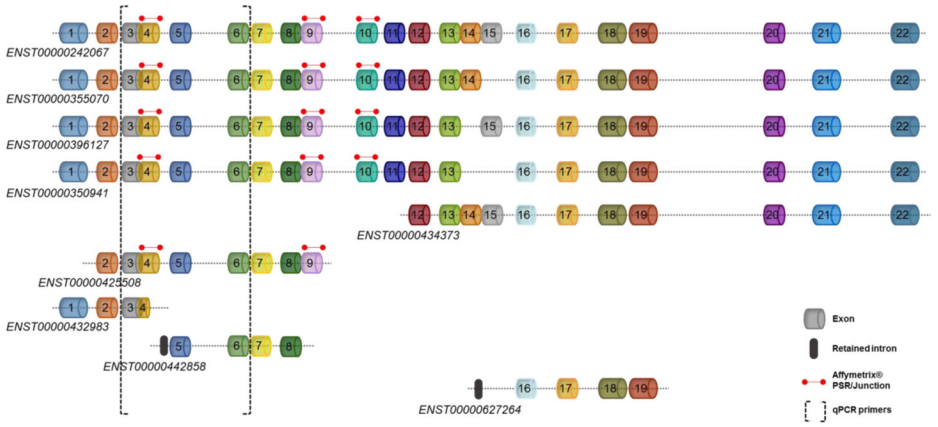

Figure 2. Alternative splice variants of the *BBS9* gene

The diagram is built based on *BBS9* sequence annotations available on the Ensemble genome browser (https://www.ensembl.org/index.html); splice isoforms that are described as coding variants are listed, with differential color coding for the different exon compositions. See text for details.

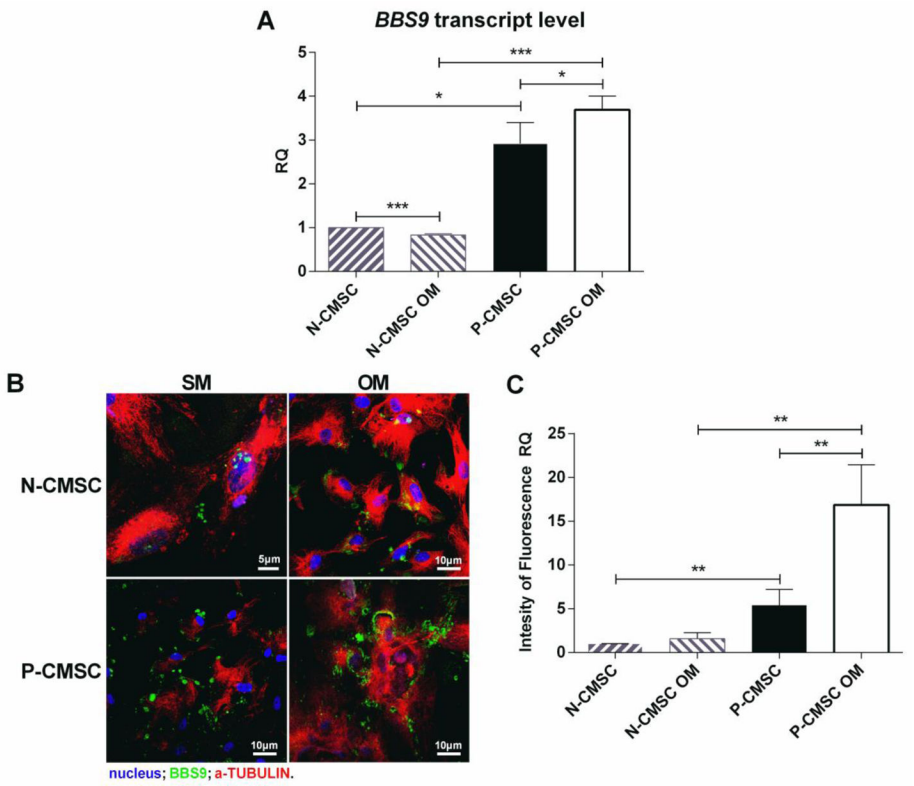

Figure 3. BBS9 expression analysis

(*A*) The expression of the specific *BBS9* splice isoforms (see text and Figure 2 for details) was analyzed by qPCR in N- and P-CMSC, cultured in either standard growth medium (SM) or in osteogenic medium (OM). Relative quantity (RQ) was calculated according to the ΔΔCt method, using N-CMSC as controls in the comparison. All data are expressed as mean fold change ± standard deviation (SD) across replicates. Unpaired t-test was used to detect the statistical significance between samples; *p≤0.05; ***p≤0.001. (*B*) BBS9 expression and localization in N- and P-CMSC assessed by immunofluorescence and confocal microscopy (cells grown in standard medium, SM, on left panels; cells grown in osteogenic medium, OM, on right panels). Quantitative analysis of the morphological data was performed by analyzing the intensity of the fluorescence by confocal microscopy (*C*), using N-CMSC as controls in the comparison, with value set to 1; unpaired t-test was used to detect the statistical significance between groups; **p≤0.01.

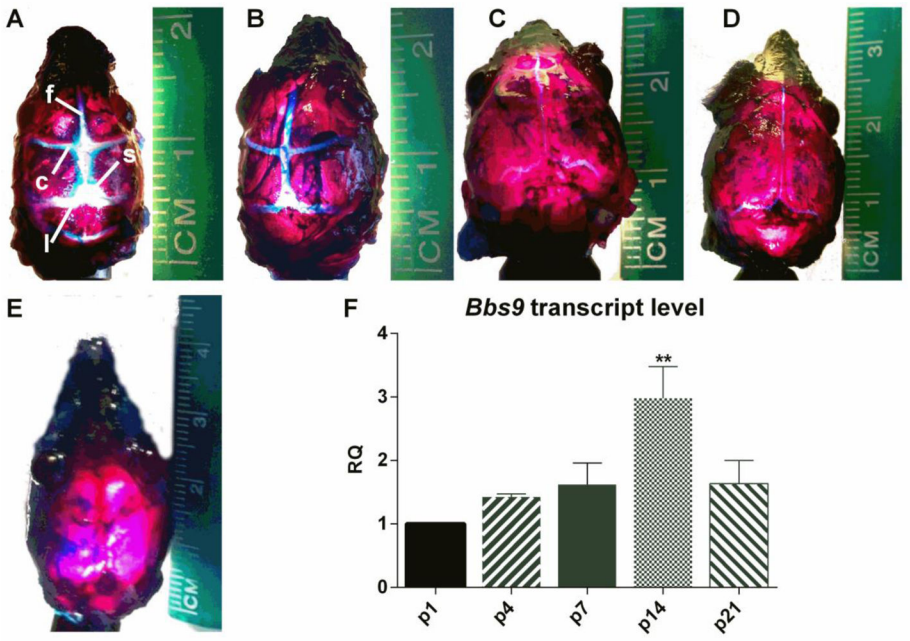

Figure 4. *In vivo* analysis of *Bbs9* expression

Whole mount staining of rat skulls at postnatal day 1 (p1; *A*), 4 (p4; *B*), 7 (p7; *C*), 14 (p14; *D*) and 21 (p21; *E*). Bony areas are stained in red with Alizarin red staining, fibrous and cartilaginous areas are stained in blue with alcian blue staining (f=frontal suture; c=coronal suture; s=sagittal suture; l=lambdoid suture). (*F*) *Bbs9* gene expression analysis during rat skull ossification. All data are expressed as mean fold change ± SD across replicates, with p1 used as control reference in the comparison (value set to 1). RQ=relative quantity. Unpaired t-test is used to detect the statistical significance between samples; **p≤0.01.

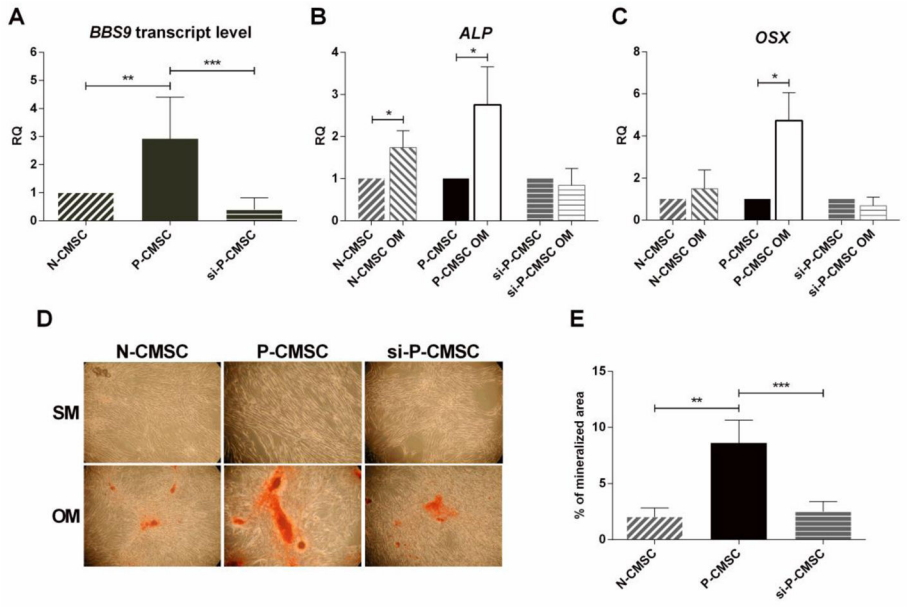

Figure 5. Effect of *BBS9* knockdown on the osteogenic potential of suture-derived cells

qPCR allowed assessing the expression of BBS9 (*A*), *ALP* (*B),* and *OSX* (*C*), in N-. P- and si-P-CMSC, grown in OM compared with standard growth conditions. The acquisition of an osteogenic phenotype was assessed by Alizarin red staining for mineralized matrix deposition (*D*). The results of quantitative evaluation of mineralized matrix deposition by Alizarin red staining are shown in the graph in N-, P- and si-P-CMSC after osteogenic induction (*E*); the extent of mineralized area is expressed in percentage. Unpaired t-test is used to detect the statistical significance between the tested groups; *p≤0.05; **p≤0.01; ***p≤0.001.

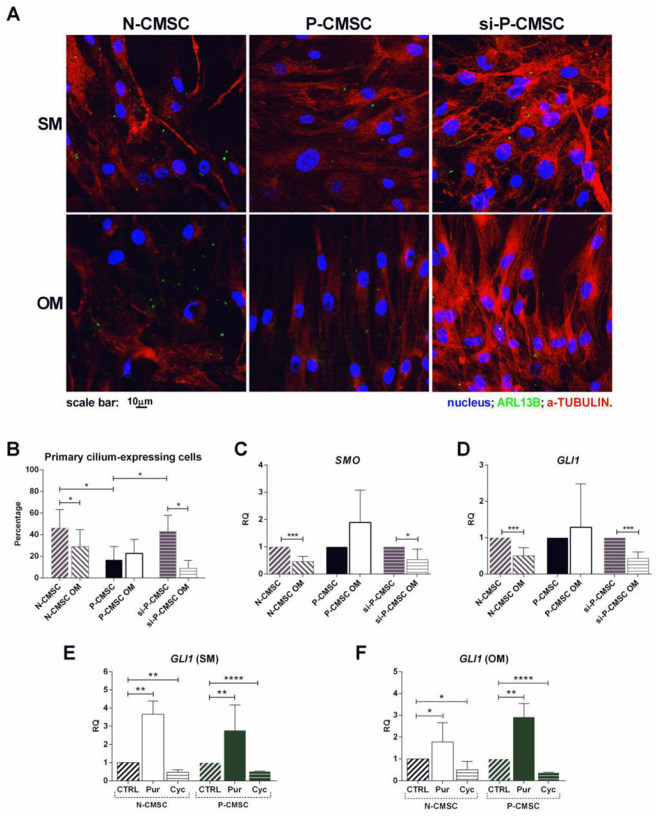

Figure 6. Effect of *BBS9* knockdown on primary cilium expression

Confocal microscopy allowed detecting primary cilium-expressing cells in N-, P-, and si-P-CMSC cultures (*A*). SM: cells grown in standard growth medium (upper panels), OM: cells grown in osteogenic medium (bottom panels). The percentage of primary cilium-expressing cells is showed in the histogram in (*B*). (*C. D*) The expression of *SMO* and *GLI1* genes was assessed in N-, P- and si-P-CMSC, grown in OM or SM, by qPCR (see text for details). *(E, F)* The expression of *GLI1* gene was assessed in N- and P-CMSC grown in OM or SM in presence of Purmorphamine (Pur) or Cyclopamine (Cyc), alternatively, by qPCR (see text for details). Unpaired t-test was used to detect the statistical significance between groups; *p≤0.05; **p≤0.01; ***p≤0.001; ****p≤0.0001.

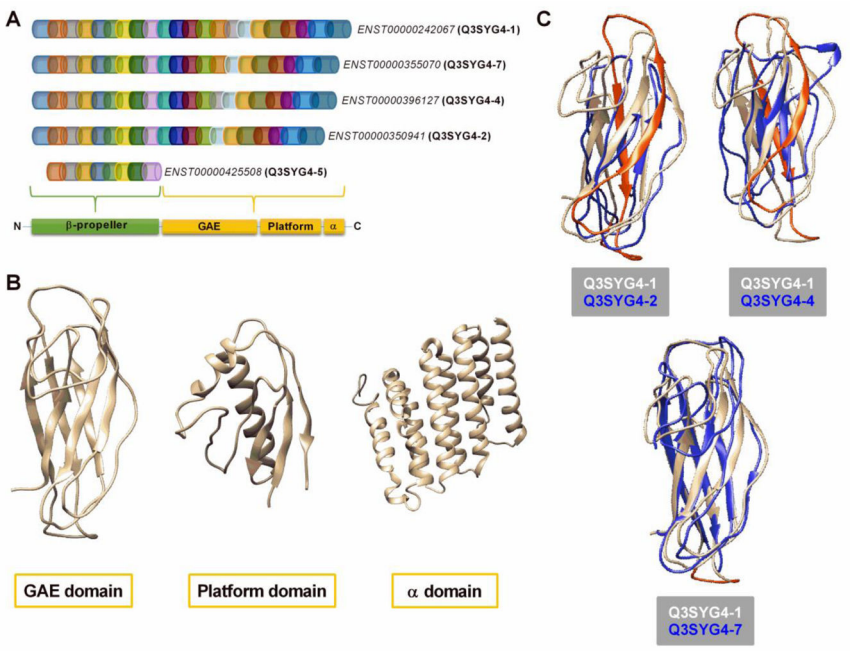

Figure 7. Computational modeling of the secondary structures of BBS9 protein isoforms

(*A*) The uppermost schemes display the sequence of exons (color codes as shown in Figure 2), composing the full-length and the alternatively spliced transcripts of the *BBS9* gene; the lowermost diagrams hows the organization of protein domains in the secondary structure (see text for details). (*B*) The diagrams show the predicted tertiary structures for GAE, platform and α domains of the BBS9 protein isoform Q3SYG4-1 (translated from the *ENST00000242067* splice variant). *(C)* The result of structure-based alignment of the full length Q3SYG4-1 (colored in white) compared with the alternative GAE domains of the selected BBS9 isoforms (colored in blue) (see text for details). In each diagram, the peptide structure corresponding to the nucleotide sequence that is skipped in the spliced isoforms is colored in red.